











Article

Evaluation of Coastal Sediment Dynamics Utilizing Natural Radionuclides and Validated In-Situ Radioanalytical Methods at Legrena Beach, Attica Region, Greece

Christos Tsabaris ^{1,*}, Alicia Tejera ², Ronald L. Koomans ³, Damien Pham van Bang ⁴, Abdelkader Hammouti ⁴, Dimitra Malliouri ¹, Vasilios Kapsimalis ¹, Pablo Martel ², Ana C. Arriola-Velásquez ², Stylianos Alexakis ¹, Effrosyni G. Androulakaki ¹, Georgios Eleftheriou ¹, Kennedy Kilel ⁵, Christos Maramathas ⁶, Dionisis L. Patiris ¹ and Hannah Affum ⁷

- ¹ Hellenic Centre for Marine Research, Institute of Oceanography, 46.7 Km Athens-Sounio Ave., 19013 Anavyssos, Greece; d.malliouri@hcmr.gr (D.M.); kapsim@hcmr.gr (V.K.); salexakis@hcmr.gr (S.A.); e.androulakaki@hcmr.gr (E.G.A.); geoelefthe@hcmr.gr (G.E.); dpatiris@hcmr.gr (D.L.P.)
- ² Physics Department, Institute of Environmental Studies and Natural Resources, Universidad de Las Palmas de Gran Canaria, 35017 Las Palmas de Gran Canaria, Spain; alicia.tejera@ulpgc.es (A.T.); pablo.martel@ulpgc.es (P.M.); ana.arriola101@alu.ulpgc.es (A.C.A.-V.)
- ³ Medusa Explorations BV, Skagerrak 26, 9723 JR Groningen, The Netherlands; ronald@medusa-online.com
- ⁴ Department of Construction, Ecole de Technologie Supérieure Université du Québec, ETS, 1100 rue Notre-Dame Ouest, Montréal, QC H3C 1K3, Canada; damien.pham-van-bang@etsmtl.ca (D.P.v.B.); a.hammouti@etsmtl.ca (A.H.)
- ⁵ Department of Physics, Kenyatta University, Nairobi 00100, Kenya; kilel.kennedy@ku.ac.ke
- ⁶ teleDOS Laboratories S.M. P.C. - teleDOS Nuclear Tech, 20131 Corinth, Greece; cmaramat@teledos.eu
- ⁷ Radiochemistry and Radiation Technology Section, Division of Physical and Chemical Sciences, Department of Nuclear Science and Applications, International Atomic Energy Agency (IAEA), A-1400 Vienna, Austria; h.affum@iaea.org
- * Correspondence: tsabaris@hcmr.gr; Tel.: +30-2291-0764-10



Academic Editor: Gianluca Quarta

Received: 19 May 2025

Revised: 16 June 2025

Accepted: 23 June 2025

Published: 26 June 2025

Citation: Tsabaris, C.; Tejera, A.; Koomans, R.L.; Pham van Bang, D.; Hammouti, A.; Malliouri, D.; Kapsimalis, V.; Martel, P.; Arriola-Velásquez, A.C.; Alexakis, S.; et al. Evaluation of Coastal Sediment Dynamics Utilizing Natural Radionuclides and Validated In-Situ Radioanalytical Methods at Legrena Beach, Attica Region, Greece. *J. Mar. Sci. Eng.* **2025**, *13*, 1229. <https://doi.org/10.3390/jmse13071229>

Copyright: © 2025 by the authors. Licensee MDPI, Basel, Switzerland. This article is an open access article distributed under the terms and conditions of the Creative Commons Attribution (CC BY) license (<https://creativecommons.org/licenses/by/4.0/>).

Abstract

This study was realized in the frame of an IAEA Coordinated Research Project for the evaluation of sediment dynamics, applying in-situ radiometric methods accompanied with a theoretical model. The in-situ methods were validated using lab-based high-resolution gamma-ray spectrometry. Sediment dynamics assessments were performed based on the measured and mapped activity concentrations of specific ²³⁸U progenies (²¹⁴Bi or ²¹⁴Pb), ²³²Th progenies (²⁰⁸Tl and ²²⁸Ac), and ⁴⁰K along the shoreline of the beach. The maps of the activity concentrations of natural radionuclides were produced rapidly using software tools (R language v4.5). The sediment dynamics of the studied area were also investigated through numerical simulations, applying an open source model considering land–sea interactions and meteorological conditions and the corresponding sediment processes. The assessments, which were conducted utilizing the detailed data from the natural radioactivity maps, were validated by the simulation results, since both were found to be in agreement. Generally, it was confirmed that the distribution of radionuclides reflects the selective transport processes of sediments, which are related to the corresponding processes that occur in the study area. Legrena Beach in Attica, Greece, served as a pilot area for the comparative analysis of methods and demonstration of their relevance and applicability for studying coastal processes.

Keywords: beach sand; in situ instrumentation; natural radionuclides; sediment dynamics; erosion-accretion; radioactivity mapping; rapid maps; protected marine areas

1. Introduction

The radioactivity levels of Naturally Occurring Radionuclides (NOR) exhibit spatial and temporal gradients due to the geochemical composition and geophysical conditions of the Earth's crust, which affect geological materials such as sediments, sands, and rocks, which, under certain circumstances, can be considered as naturally occurring radioactive material (NORM) [1]. NOR are also typically reported in the literature to support efforts to characterize aquatic systems. Recent studies have focused on determining the activity concentration of natural radionuclides in sediments to assess sediment transfer in river systems, as well as to reconstruct historic flooding events using thorium isotopes as radio-tracers [2,3]. Other studies have focused on the use of natural radionuclides in sediments as tracers for identification of transport pathways in coastal areas [4–6].

Recent changes in the mass balance of closed and semi-closed marine systems may result in natural variability of the morphology of the seashore coastline. In this context, an improved understanding of the long-term changes in sediment behavior is essential, to better understand the internal and external environmental parameters and laws that govern sediment dynamics' processes. The concentrations of NOR can vary in sediments due to their provenance [7,8], and their potential to act as a sink and source of radionuclides in the marine environment. Land–sea interactions and runoff from terrestrial ecosystems may add soluble material in surface sediments or partially remove them. As is the case for the elemental composition, the radionuclide composition of the sediment in a certain position on a beach can vary due to an influx of matter with flood waters (e.g., river- and stream-borne particles), or due to processes which sort the sediments by their grain size and density [9,10].

One of the major objectives of this work was to validate the use of portable gamma detection systems for studying sediment dynamics in a beach area in situ, using natural radionuclides as tracers, i.e., to study sediment transport phenomena influenced by marine dynamics (mainly wave action and its interaction with beach morphology). More specifically, an attempt to correlate the distribution of sediments with their radionuclidic content was made, since the sediment dynamics' evaluation was performed through the detailed maps of activity concentrations of natural radionuclides in a protected marine coastal area, "Legrena Beach". The maps were produced by spatial gamma scanning using three portable radioactivity analysis systems (two identical KATERINA II gamma spectrometry systems and one MS-350 MEDUSA system). The KATERINA II systems [11–14] were installed in a backpack configuration as well as in a dedicated trolley. The MEDUSA system was mounted on a backpack [2,5]. The two activity-quantification methods, one applied with KATERINA II systems and another one with MEDUSA, were validated using high-resolution lab-based gamma-ray spectrometry (HRGS) [15]. The sediment dynamics and related processes that have taken place at "Legrena Beach" were evaluated by comparing the distribution of NOR in the sediment with a sediment transport model for this site (computational simulations, involving the application of an existing model taking into account land–sea interactions, meteorological conditions, and corresponding sediment processes). The assessments, which were conducted utilizing the detailed data from the natural radioactivity maps, were validated by the simulation results, since both were found to be in agreement.

2. Study Area

The study area (Legrena Beach) is situated in the Attica region east of Sounio on the coast of the Attica Peninsula (see Figure 1a). Legrena Beach, a pristine sandy beach, is nestled 60 km from Athens and 3 km from the historic Cape Sounion. The beach area is open to dominant southwestern winds, which can become very strong a few times during

the year, causing large waves. Its main characteristics are fine sand, small bushes, dunes and crystal-clear blue waters. The water deepens gradually, having a depth of 5 m at a distance of 10 m from the shoreline. The water temperature during the year varies from 14 degrees in January up to 28 degrees in July, August, and September. December and February receive the highest rainfall, with the precipitation amount reaching the level of 65.4 mm. Additionally, the relative humidity during the same period is close to 72%. Regarding the area morphology, Legrena Beach is a semi-open beach, exposed to wave action in its central area, and protected on both the eastern and western sides by a semi-submerged rocky bar. On the westernmost side, this protection is more pronounced due to the longer rocky bar and, primarily, the presence of a marina at this boundary.

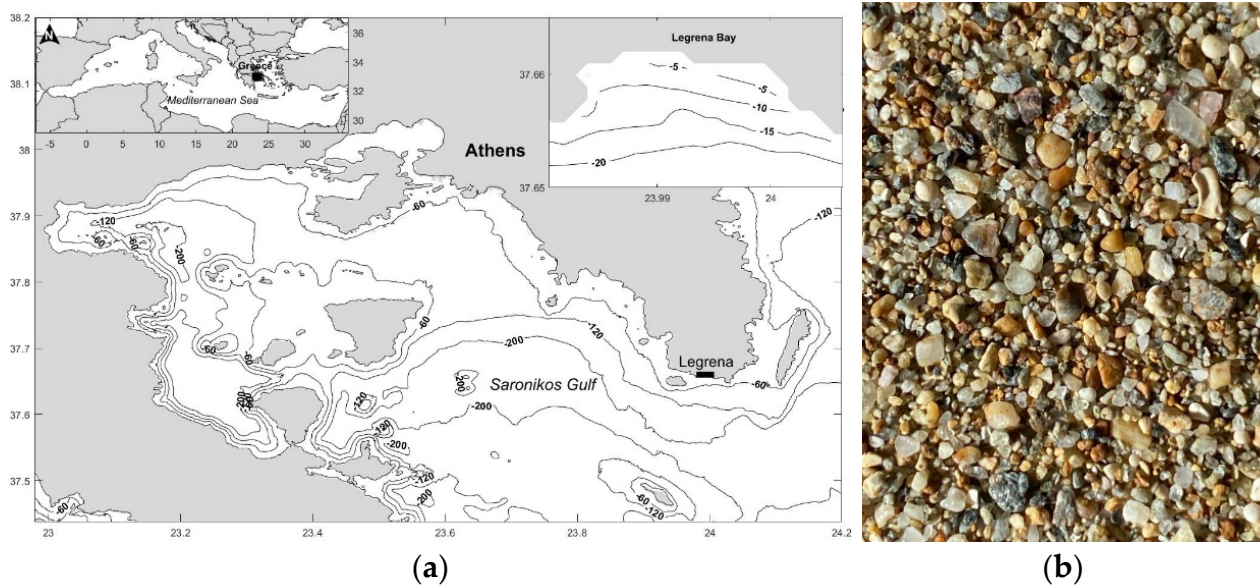


Figure 1. (a) Map of the wider study area in Legrena (Attica region, Greece); (b) Typical sediments found on Legrena Beach.

One of the unique characteristics of Legrena Beach is its natural protection status without enhanced anthropogenic interactions during the last 30 years, since the construction of the marina in 1980. Legrena Beach is considered a protected marine area and is not affected by anthropogenic activities. A lot of efforts have been made to keep this beach as an ideal clean place for maintaining biodiversity and coastal resilience processes. The beach is affected (especially during winter) by south-east winds moving sand towards the village of Legrena. A large amount of sand is bounded in the dunes of the coastal system, preserving the stability of the shoreline. The sediment type at this location is composed of a mixture of poorly sorted sediments with well-rounded and angular grains, showing rock fragments, quartz particles, and some shell fragments (see Figure 1b).

3. Materials and Methods

3.1. KATERINA II Detection System

The KATERINA II underwater detection system [11,12,14] was initially developed to continuously monitor the level of radioactivity in the oceans [16,17], and the levels of radon and thoron progenies in water resources (e.g., submarine groundwater discharges and springs). KATERINA II consists of a $3'' \times 3''$ NaI(Tl) scintillator coupled with a photomultiplier tube and a preamplifier combined with appropriate units for signal amplification, stabilization, digitalization, data acquisition, and storage, all sealed in a special lightweight, watertight, and pressure-proof housing, capable of continuously withstanding harsh conditions when in underwater, ground, or aerial use. The electronic modules have a low power

consumption (~ 1.0 W), which makes the detection system suitable for remote applications. The system is designed to be easily integrated into any fixed station, floating, and/or mobile platform, allowing it to operate in stand-alone as well as in near real-time data transmission mode.

The KATERINA II detection system is upgraded to perform rapid gamma-ray spectrometric measurements in a spatial scanning mode, since a mini-GPS module is integrated; therefore, geo-referenced information is acquired and recorded simultaneously with the spectra. The detection system is programmed via a mini-computer to provide sequential time-series measurements. During the present radioactivity mapping experiments, the first configuration option was the installation of the system in a backpack, enabling all the members of the surveyors' team (workshop participants) to carry it sequentially for scanning the entire extended area of study. The second configuration was the installation of the KATERINA II system in a dedicated trolley, where the distance of the crystal from the ground (beach sand) was maintained almost constant (1 m). The trolley configuration is illustrated in Figure 2.



Figure 2. The trolley configuration where the KATERINA II geo-referenced detection system is installed together with the other modules (**upper photo**) and a surveyor carrying a MEDUSA sensor (**lower photo**).

The power was supplied by a mini battery loaded in the backpack or on the trolley. Finally, a new method of efficiency calibration was applied, and the resulting calibration factors were integrated into the full energy peak analysis/mapping software of the system. Hence, the spatial distribution of the activity concentrations of each detected gamma-ray emitter of interest can be expressed in the SI units of Bq kg^{-1} on the corresponding radioactivity maps. This new method involved well-designed extended Monte Carlo simulation runs using mainly EGSnrc MC Simulation code. The activity concentration of the gamma-ray emitters of interest was calculated using simulation values of the full energy photo-peak efficiency as produced by a model developed using the aforementioned simulation code. The validation of these values was performed using lab-based measurements by sampling beach sand from the same area of the in situ measurements. More details are given elsewhere [18]. The uncertainty budget was also calculated, taking into account the counting statistics and the efficiencies' uncertainty where geometry, density, nuclear data, counting, and other uncertainties are involved.

The mapping of the KATERINA II measurements was performed using the Inverse Distance Weighted (IDW) deterministic interpolation method. The main underlying concept is "Tobler's first law of geography", which applies to the influence of neighbor points on the total count rate (TCR) value of a selected point, where its estimation is more influenced by its neighbor points than by its distant points. The production of the maps and the calculations resulted from the use of code written in the R language [19], which provides a wide variety of statistical and graphical techniques under the terms of the Free Software Foundation's GNU (General Public License).

3.2. MEDUSA Detection System

The Medusa Radiometrics MS-350 [2,5] is a lightweight and robust gamma-ray sensor developed for walking surveys and unmanned aerial vehicle (UAV) applications. These systems are fully self-contained as they integrate data acquisition, processing and storage into a single embedded system. The MS-350 is operated from a smartphone or tablet PC using the Medusa Detector Operation System (mDOS). The system comprises a 3×3 inch (350 mL) CsI-based scintillation detector connected to a tailor-made spectrum processing unit. This unit contains a 4096-channel MCA, an RTK-ready GPS, real-time data processing, and embedded storage. The system works as a stand-alone unit, and the data can be viewed by connecting it to the interface via WiFi or ethernet on a cabled connection. The unit runs the Medusa Detector Operation System (mDOS) that provides access to the multiple functions of the device:

- Set-up of the system;
- Status view to inspect data and functioning of the system;
- Single and continuous measurement modes;
- View the data in real time plotted on a map;
- Download data for custom post-processing.

The data is stored in records containing energy-stabilized gamma-ray spectra. These spectra were analyzed for the activity concentrations of ^{40}K , and gamma-ray emitters of ^{238}U and ^{232}Th progenies and ^{137}Cs using full spectrum analysis. This approach fits the spectral response curves of the concentrations of 1 Bq kg^{-1} of the aforementioned gamma-ray emitters to the measured spectra. The response curves were determined by Monte Carlo simulations and a detector-specific efficiency calibration in the Stonehenge calibration facility [20]. The data was geo-referenced using the built-in GPS, the maps of the MS-350 system were made in QGIS 3.22, and the interpolations were performed in Surfer (Golden Software 26) based on kriging [21].

3.3. High Resolution Gamma-Ray Spectrometry Analysis

The validation of the in-situ methods was carried out through a sampling process in the study area and subsequent measurement analysis using high-resolution gamma-ray spectrometry. Before performing the in situ mapping of natural radioactivity, sand samples were collected to determine the activity concentrations along the coastline. A total of 16 were collected in November 2023 (Figure 3) from Legrena Beach, specifically from near-surface sediments (0–5 cm) on the beach and at the beach–sea interface (several meters from the berm area of the beach). Samples were collected from the intertidal zone during low tide to enhance the understanding of marine hydrodynamics and facilitate a comprehensive assessment of intertidal sedimentary processes influenced by marine action. At each sampling point, a 1 m² area was marked, and superficial sand samples were collected from the top 0–5 cm of the sediment after being homogenized in-situ (Figure 4a). Once the samples were transferred to the laboratory, they were dried at 80 °C for 24 h, sieved through a 1 mm mesh for homogenization, and stored in PVC containers sealed with aluminum strips to prevent radon gas escape (the containers were filled in a way to prevent a void air space above the sample matrix), therefore enabling an “as accurate as possible” ²²⁶Ra determination through its gamma-emitting progenies [22,23]. The samples were then stored for one month to allow secular equilibrium between ²²⁶Ra and its progenies, ensuring reliable measurement conditions. The prepared sand samples were analyzed using a Low-level Extended Range (XtRa) Germanium Spectrometer (Figure 4b), calibrated with Monte Carlo methods which were verified against reference materials (e.g., IAEA RGK-1, RGU-1, and RGTh-1) [24].



Figure 3. Sampling points at Legrena Beach, selected for beach sand samples’ collection and radiological characterization through the lab-based HRGS analysis.

Specific gamma emission energy lines were recorded in the spectra, and the corresponding photopeaks were used to quantify the activity concentration of radionuclides in Bq kg^{−1}. The photopeak at 351.93 keV of ²¹⁴Pb was used to determine the activity concentration of ²²⁶Ra. The emission line at 911.19 keV corresponding to ²²⁸Ac was used to obtain the activity concentration of ²²⁸Ra. The line at 1460.82 keV is directly associated with ⁴⁰K. Each sample was measured for 24 h to determine the activity concentration values with high precision [24]. The counting statistics, the uncertainty from the continuum and peaked background subtraction, and the uncertainty of the true-coincidence correction, as well as the efficiencies’ and nuclear data uncertainties were all included in the uncertainty budget and the combined uncertainties were calculated accordingly.

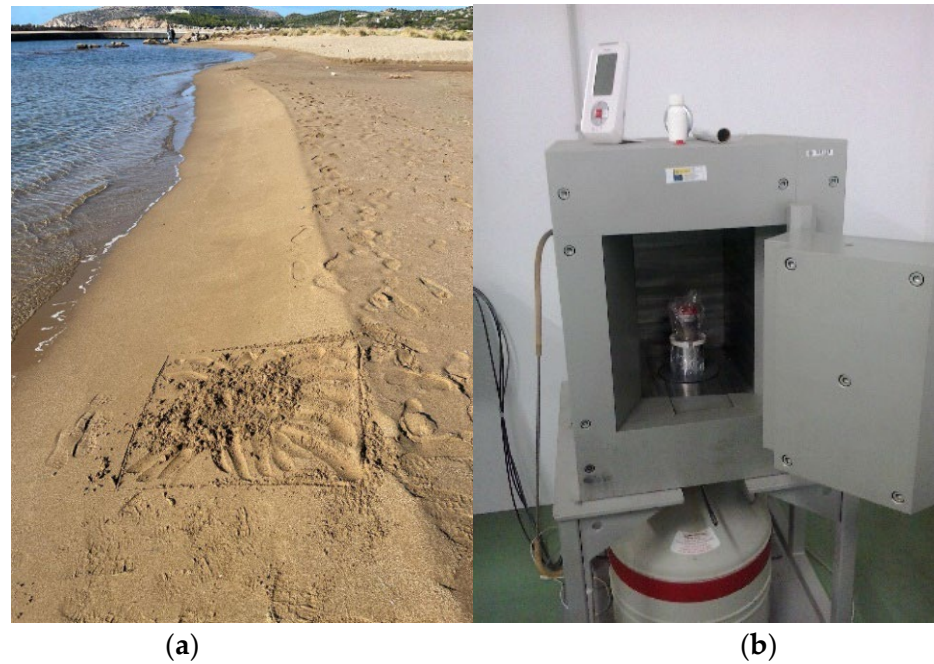


Figure 4. (a) A sampling point after sand sample collection, as selected in the intertidal zone in Legrena Beach (left); (b) low-level high-resolution gamma-ray spectrometer comprised of a shielded Extended Range (XtRa) Germanium detector (right).

3.4. Numerical Coastal Model of Legrena Bay

3.4.1. Shoreline Evolution and Topo-Bathymetric Data

For the period 1945–2023, shoreline observations of Legrena Beach from aerial (Hellenic Military Geographical Service) photographs and satellite (Google Earth) images have been collected for analyses on coastline evolution during the two construction phases of the marina. Figure 5 presents the results, showing a general coastal retreat tendency of the site: the retreat of the coast is higher in the eastern part of the marina, with a maximum around 28 m (point E) for the past 78 years.



Figure 5. Shoreline detection in satellite imagery for the study time period: 1945 to 2023. The different coastal areas are represented by letters from A to F.

The geomorphological information of the Legrena site is obtained from the available topometric and bathymetric data of the Hellenic Centre for Marine Research. These different data (land cover by Lidar, coastal and offshore zones by mono- or multibeam sonar) are merged to generate a full topo-bathymetry file. The computational domain ($1900 \text{ m} \times 1200 \text{ m}$) is bounded by two headlands forming the Legrena pocket beach. The offshore boundary is 1200 m from the marina. In the present study, it is assumed that the offshore boundary is sufficiently far from the marina in order to neglect the influence of boundary conditions on the wave results near the shoreline. The unstructured triangular mesh (36,002 elements, 18,397 nodes) is considered to cover the domain, with a variable space resolution ranging from 2 m on the land surface up to 50 m at the offshore boundary.

3.4.2. Wave Conditions

Figure 6 presents the time series of wave conditions between 1 January 2020 and 30 June 2021.

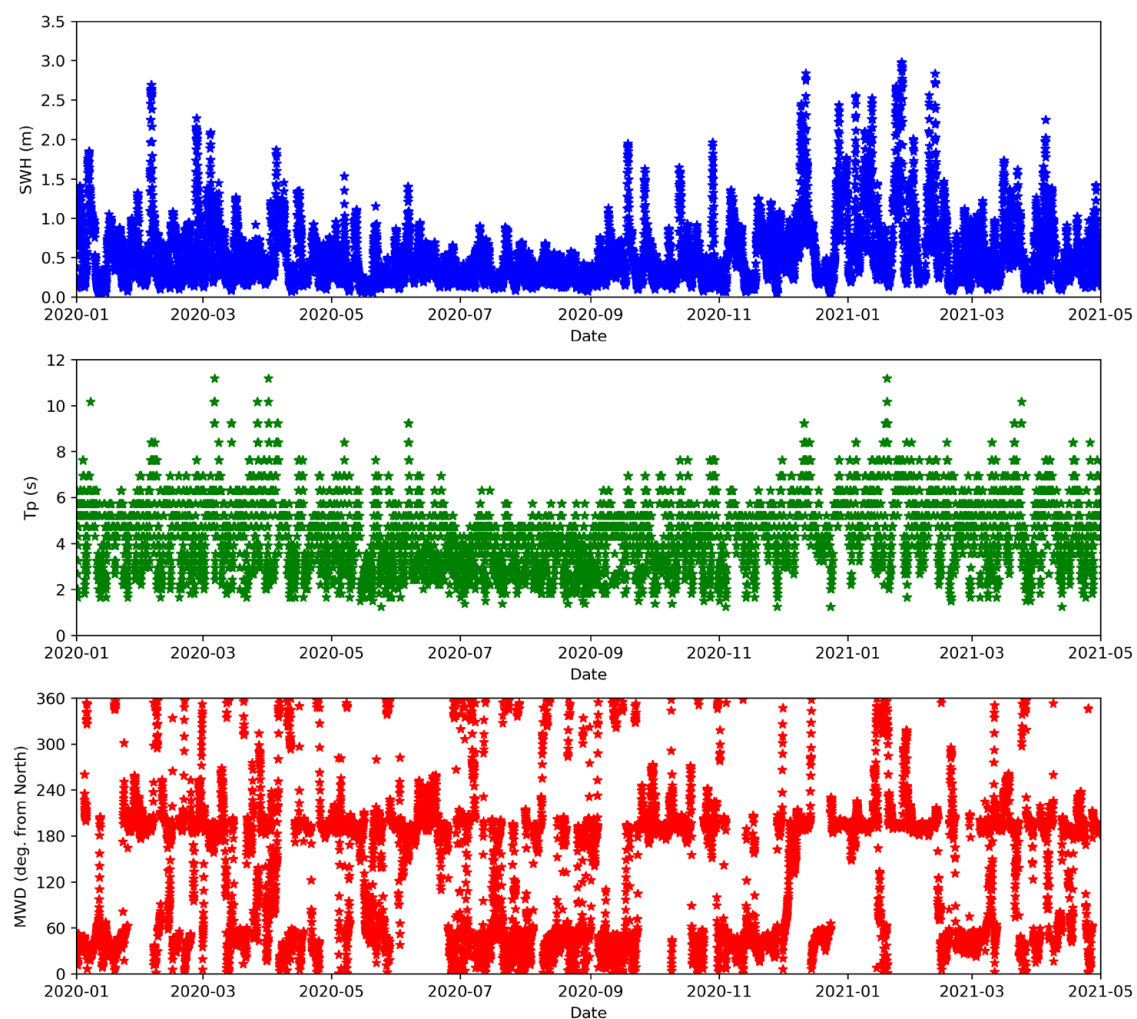


Figure 6. Wave conditions at the Legrena site during the period 1 January 2020 to 30 June 2021: the significant wave height (SWH, **up**); peak wave period (Tp, **middle**); mean wave direction (MWD, **below**) data from EU Copernicus Marine Service Information. (18 months), collected from the E.U. Copernicus Marine Service Information [25,26]. During this period, the significant wave height (SWH) varies between 0.1 and 3.0 m, the peak period (Tp) between 1.5 and 11.0 s, and the mean wave direction is 210° (i.e., coming from the southwest), while some sea states correspond to mean wave directions of 0° and 350° from the north.

3.4.3. Wave Model

The wave propagation and characteristics were computed using the finite element open-source code TELEMAC-TOMAWAC [27,28]. TOMAWAC is one wave module of the integrated suite TELEMAC that also incorporates modules for current, sediment, and morphological evolution. The modeling system is used for many applications requiring complex coupling, such as salinity and sediment transport in large estuaries [29]. TOMAWAC (hereafter TWAC) is a phase-averaged wave model which solves the unsteady evolution of the directional spectrum of wave action. In this study, coastal processes such as refraction, bottom friction dissipation, depth-induced wave breaking, and non-linear wave–wave interactions were considered. Specifically, the consideration of wave refraction is vital in order to describe the variations of wave energy at the headlands and in different areas of the Legrena bay. Referring to the offshore boundary conditions, a sea state of specific characteristics was simulated: namely, a significant wave with a H_s of 0.159 m, peak frequency of 0.159 Hz, and mean wave direction of 34.84° deg from north. Hence, a directional Jonswap spectrum was imposed, with an angular distribution function of (3), a directional spread of 3, and a peak-enhancement factor of 3.3.

4. Results

The gamma-ray surveys were performed by integrating/mounting the geo-referenced low-resolution gamma-ray spectrometers (KATERINA II-HORST Ltd/HCMR, Anavyssos, Greece and MEDUSA—Groningen, The Netherlands) in backpack and trolley modes to enable the scanning and radiological mapping of the entire study area with ease and repeatability. The recorded data are depicted as round points colored according to their respective activity level. The activity concentration maps of TCR, ^{40}K , ^{238}U progenies, and ^{232}Th progenies were calculated using the aforementioned quantification methods.

4.1. KATERINA II System in the Backpack Mode

A map of the total count rate (TCR) as well the activity concentrations of ^{40}K , ^{214}Bi and ^{208}Tl for Legrena Beach is shown in Figure 7. The TCR varied from 56 to 169 counts per s (cps) in the entire area. Upon dunes' area exclusion, the TCR variation becomes narrower, within the range 56–100 cps. In total, 392 spectra were acquired during the experiment, with an overall live time equal to 7840 s (392×20 s). After automated spectral analysis using the dedicated software which accompanies KATERINA II and utilizes the efficiency factors resulting from the aforementioned MC calibration, the activity concentration levels of ^{40}K , ^{214}Bi , and ^{208}Tl (expressed in Bq kg^{-1}) were determined. The spatial distribution of ^{40}K is depicted in the map in Figure 7.

More specifically, the activity concentration of ^{40}K varies from 104 to 194 Bq kg^{-1} , exhibiting the highest values in the dunes' area, and in the beds of a river and the streams near the eastern side of the beach, as well as at the east part of the beach. The activity concentration of ^{214}Bi varied within the range $5.4\text{--}13.0 \text{ Bq kg}^{-1}$. The highest concentrations were also found in the east part of the beach, as well as at the west part in an area where a stream is present. The variation in the activity concentration of ^{208}Tl ranged from 0.6 to 11 Bq kg^{-1} . The highest values were found at the same locations where ^{214}Bi concentration levels were high, i.e., at the east part of the beach, as well as in the vicinity of a stream at the west part. Relatively high concentrations were observed at the midpoint of the beach shoreline.



Figure 7. Map of the spatial distribution of the TCR, ^{40}K , ^{214}Bi , and ^{208}Tl as determined by the scan using the KATERINA II system in the backpack configuration.

4.2. KATERINA II System in the Trolley Mode

A map of the total count rate (TCR), using the trolley method for scanning the Legrena Beach area, is given in Figure 8. The TCR varied from 61 to 145 cps over the entire area. During the experiment, 297 spectra were acquired and the overall live time of the measurements was 5940 s (297×20 s).

The activity concentration levels of ^{40}K , ^{214}Bi , and ^{208}Tl were also determined and depicted in Figure 8. The activity concentration of ^{40}K was plotted according to the procedure already described. Figure 8 shows the spatial distribution of the aforementioned natural radionuclides. Generally, the activity concentrations of ^{40}K , ^{214}Bi , and ^{208}Tl were found to vary within the ranges 141–205, 11–15, and 8.5–13 Bq kg^{−1}, respectively. As expected, the highest concentrations for each radionuclide were located close to the parts of the beach where they were also elevated when the backpack method was applied for the scan. The local maxima for ^{40}K were recorded in the dunes' area and in the eastern part of the beach. The highest concentrations of ^{214}Bi were found at the edges of the beach (the west and the east part) and in a few points close to the dunes. The highest activity concentrations of ^{208}Tl were observed in the western part of the beach, in the vicinity of a stream, and at the eastern part.

4.3. MEDUSA System

The map of the total count rate (TCR) is shown in Figure 9 for the Legrena Beach area using the MEDUSA system for the scan. The TCR varied from 47 to 90 cps over the entire area (for inter-comparison purposes, the area in the dunes' direction was not taken into account). The activity concentration of ^{40}K varied from 90 to 185 Bq kg^{−1}, and its highest values were located in the dunes' area, and in the bed of a river near the eastern side of the beach, as well as at the east part of the beach.

In general, lower activity concentrations were observed in the western pocket of the beach, while higher concentrations were observed in the eastern part. Higher concentrations were also observed in the riverbed that streams into the beach. These patterns are similar for the three natural radionuclides of interest. Hence, the total count rate, which results mainly from the sum of their gamma emissions, is a good descriptor of the patterns in this specific study area.



Figure 8. Cont.



Figure 8. Map of the spatial distribution of ^{40}K , ^{214}Bi , and ^{208}Tl as determined by the scan using the KATERINA II system in the trolley configuration.

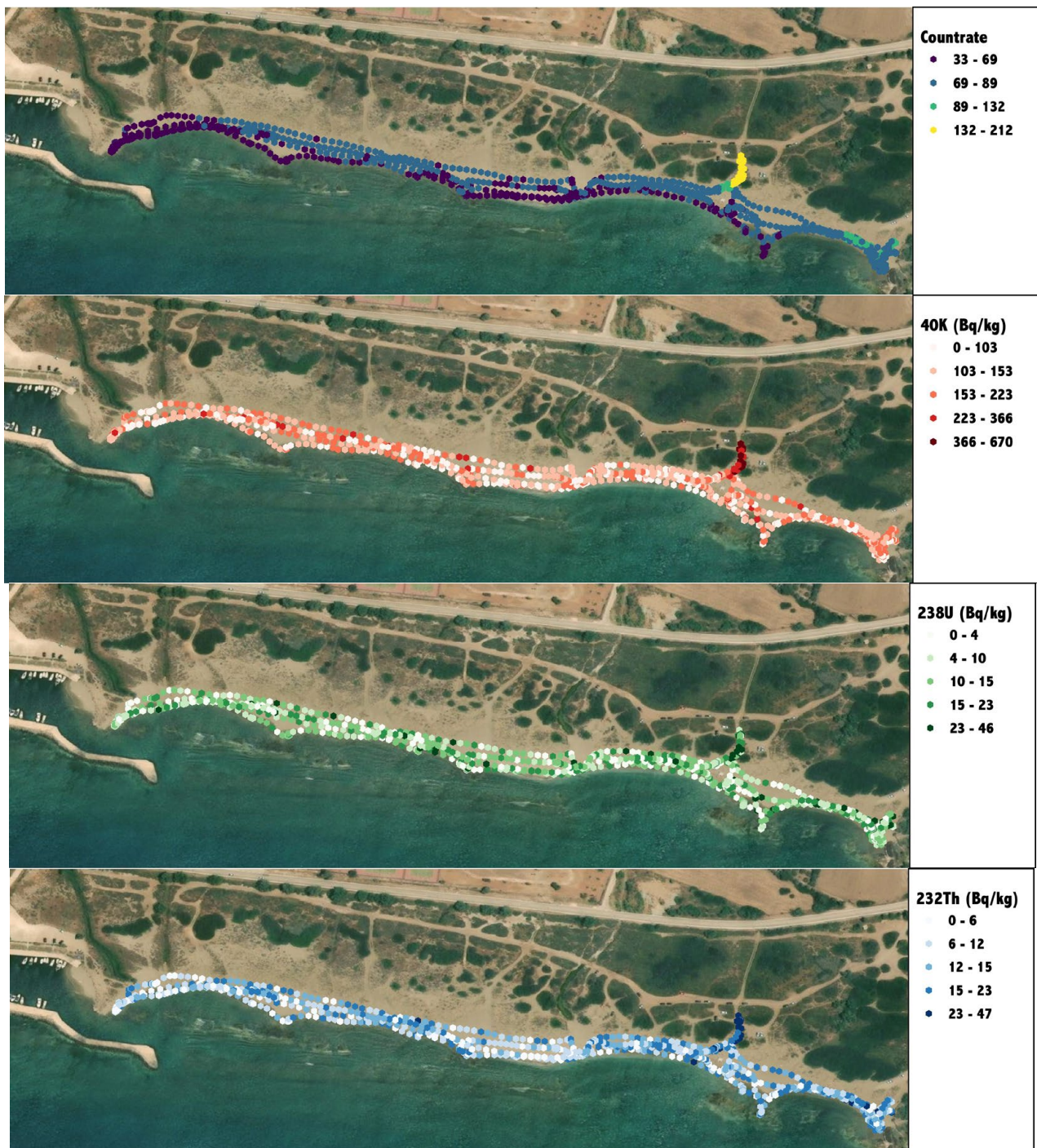


Figure 9. Maps of the ^{40}K activity concentration, the gamma-ray daughters of ^{232}Th , and ^{238}U . The graph at the bottom represents the total count rate—TCR. The experimental points are determined using the MEDUSA system in the backpack configuration. The radionuclide activity concentration is given in Bq kg^{-1} , while the TCR is given as counts per second (cps).

4.4. Validation Though Lab-Based Measurements

Each sample collected at the sampling points along Legrena Beach (Figure 3) was analyzed using HRGS. Hence, the activity concentrations of ^{40}K , $^{228}\text{Ra}/^{228}\text{Ac}$, and $^{226}\text{Ra}/^{214}\text{Pb}$ (equivalent to $^{226}\text{Ra}/^{214}\text{Bi}$) were determined for each sampling location and are plotted in Figure 10. The estimated concentrations, followed by their uncertainties (calculated at the 68% confidence level) expressed in Bq kg^{-1} , range from 31 ± 7 to 163 ± 10 , with a mean value of 102 ± 8 for ^{40}K ; from 3 ± 1 to 13 ± 2 , with a mean value of 8 ± 1 for

^{228}Ra ; and from 3.2 ± 0.7 to 8.6 ± 0.8 , with a mean value of 5.8 ± 0.7 for ^{226}Ra . The activity concentrations of ^{40}K are higher (ranging from $163 \pm 10 \text{ Bq kg}^{-1}$ to $124 \pm 8 \text{ Bq kg}^{-1}$) at the sampling points (P3, P4, P5, P6, P7, and P16) located in the western section and the easternmost end of the beach. In contrast, the lowest values (ranging from $31 \pm 7 \text{ Bq kg}^{-1}$ to $73 \pm 7 \text{ Bq kg}^{-1}$) are found at the P8, P9, P10, P11, and P12 stations, situated in the central part of the beach.

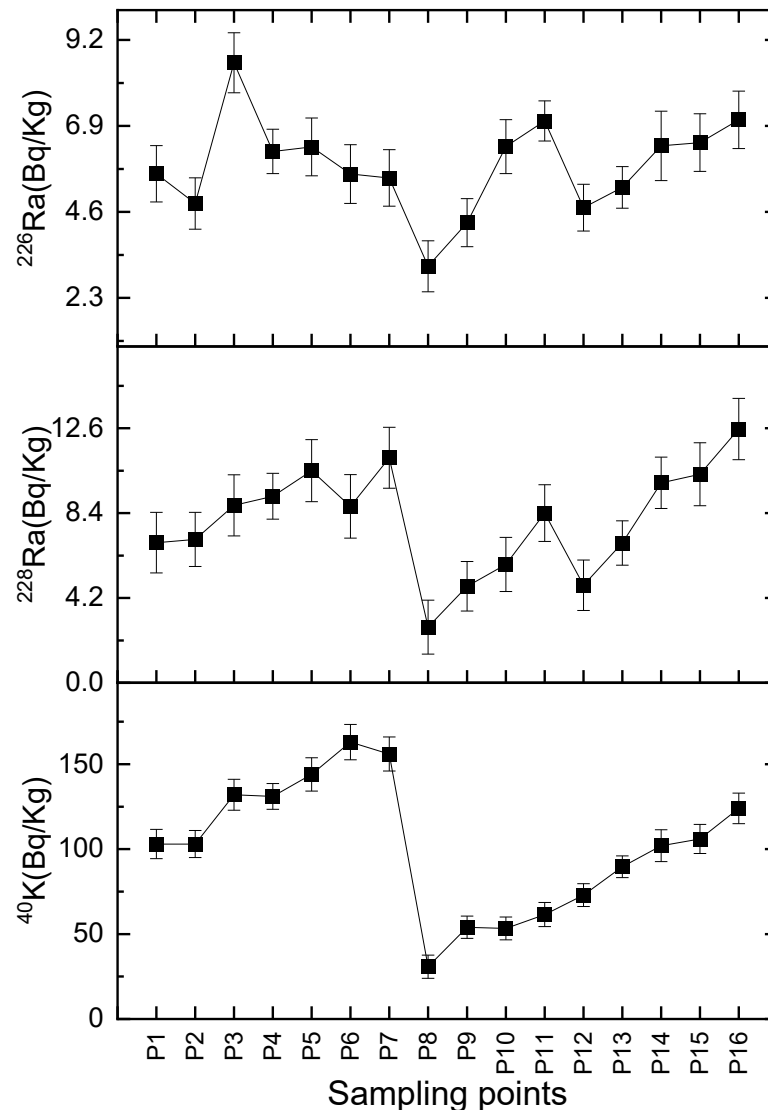


Figure 10. Results of the lab-based determination of the activity concentration of ^{40}K , ^{226}Ra , and ^{228}Ra at each sampling location. The sampling points are depicted in Figure 3.

Areas with the highest concentrations of ^{40}K ($163 \pm 10 \text{ Bq kg}^{-1}$) are primarily found in the zone protected by the dock dike (P3, P5, and P6, as given in Figure 3). The higher concentration of ^{40}K may be due to the selective sorting of sediments, such as feldspars and micas. These same regions also show elevated levels of ^{226}Ra ($8.6 \pm 0.8 \text{ Bq kg}^{-1}$) and ^{228}Ra ($10.5 \pm 1.5 \text{ Bq kg}^{-1}$). In Legrena Beach, the sediments are predominantly composed of medium- to coarse-grained sands that are poorly sorted in a combination of well-rounded and angular grains. The sediment is composed of rock fragments, quartz particles, particles of feldspar and some shell fragments. Higher activity concentrations of ^{40}K are associated with sediments with increased concentrations of K-feldspar particles (often lighter and fine-grained) [10,24,30]. These results agree with those obtained in the literature [15,24],

where the highest activity concentration of ^{40}K , as well as the greater presence of potassium feldspar, were related to sediments' accumulation zones.

4.5. Wave Properties

4.5.1. Significant Wave Height

Figure 11 presents the unstructured grid which has been used in the TWAC simulation of wave transformations in Legrena Beach. Regarding the simulated sea state (as described in the previous section), higher significant wave heights are estimated near zones C, D, and E, while lower values are estimated in zones A and B. In particular, zone A is a shadow zone of wave energy behind the western headland. Additionally, wave energy tends to increase eastward from A to E along the shoreline, whereas it tends to decrease from zone E to the east boundary, with a few higher, very local wave energy conditions in zone F.

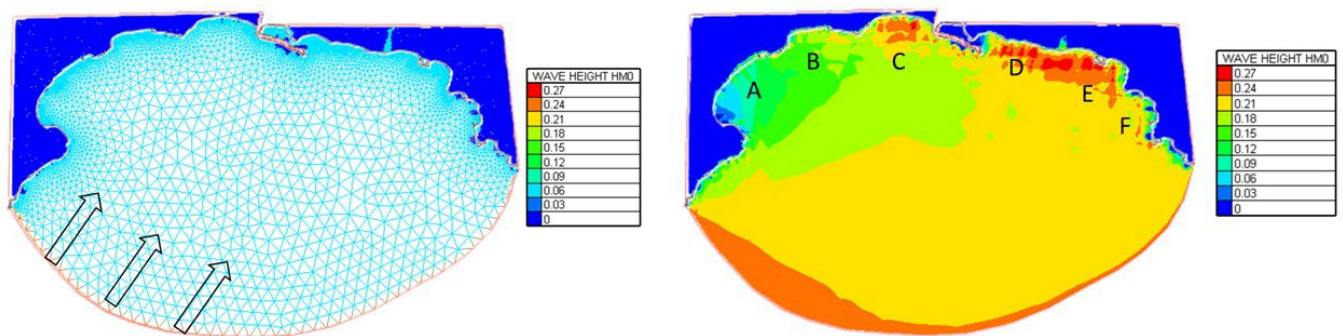


Figure 11. Spatial distribution of significant wave height: unstructured triangular computational grid (2–50 m resolution, **left**) with the main wave direction; significant wave height results from the TWAC model (**right**).

4.5.2. Wave Refraction Pattern

Results on the spatial distribution of the mean wave direction are illustrated in Figure 12, corresponding to the offshore mean wave direction of 34.84° from the north. Particularly, the derived results reveal the increasing tendency of wave rays to become perpendicular to the shore as waves propagate from deep waters onshore, due to refraction effects. Because of the parabolic headland-bay shape, a shadow wave energy region is met at the western headland, whilst the eastern coastal zone is exposed to higher wave energy conditions.

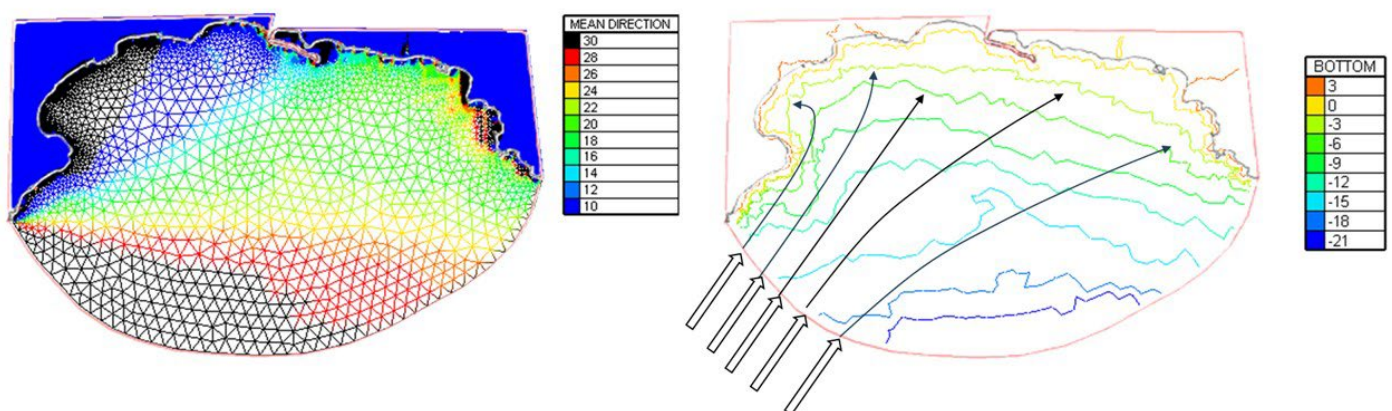


Figure 12. Distribution of wave directions: results from TWAC (**left**); schematic representation of wave refraction under non-normal wave direction (**right**).

Results on the wave refraction pattern (see Figure 12) also tend to reveal that the Legrena shoreline can be divided into two distinct regions on either side of the marina. At the western side, there is a strong refraction of wave rays, whereas at the eastern side, wave rays are smoothly refracted, characterized by higher wave energy. These findings seem to corroborate with the observation of shoreline retreat (see Figure 5) and give an insight into the fact that the shoreline segment AC records less retreat than the segment DF. Moreover, similar wave transformation processes localized near the marina can also explain the shoreline propagation in the sheltered zone (P1–P7) and the shoreline retreat in the vulnerable zone (P8–P16).

5. Discussion

5.1. Comparison Between In Situ and Lab-Based Methods

The first comparison is realized between the two scan-mode configurations of the KATERINA II systems. The two systems are identical in terms of crystal size, electronics, housing dimensions, and materials. However, the two measurement geometries are slightly different because the trolley configuration keeps the system at a constant height above ground, and there is no influence of the operator's body (soft-shielding) and height (backpack holding position). Despite these differences, the two scanning methods—backpack and trolley—were found to be in agreement or equivalent in terms of the total count rate results. Thus, excluding the data acquired in the dunes, the TCR is within the range of 56 to 100 and 61 to 105 cps, respectively; therefore, also taking uncertainties into account, there is no detectable significant difference between the scan results. Regarding the mapping of ^{40}K , the comparison of the two methods revealed a slight difference between the lower limits of the ranges of the activity concentrations. The activity concentration varied within the ranges of 105 to 196 and 141 to 205 Bq kg^{-1} , for the backpack and trolley scan, respectively; therefore, the minimum activity concentration is lower in the case of the backpack mode scan. This difference may be attributed to the fact that the trolley did not pass over beach areas where the activity concentration of ^{40}K is relatively low, while the surveyors scanning with the backpack method did, because they could walk easily over the entire area and were even able to reach rugged locations. Compatible results between the two scanning modes were also observed for the ^{214}Bi and ^{208}Tl activity concentrations.

Another interesting comparison is realized between the KATERINA II and MEDUSA systems (both in the backpack configuration). Although they are not identical—in terms of crystal type as well as electronics—and their above-ground/beach sand positions and transects were different during the scans, the data exhibited very good agreement within statistical uncertainty for the total count rate, since the TCR values, as recorded by each system, were dispersed within the ranges 56–100 and 47–90 cps, respectively. The compatibility of the results [31] of the two systems is also evident by comparing the respective spatial distributions of the activity concentration of ^{40}K : the two independent ^{40}K -maps, produced using the KATERINA II and MEDUSA detection systems, exhibit data intervals from 105 to 190 and 90 to 185 Bq kg^{-1} , respectively. In this case, the minima of the two intervals as well as the maxima are equivalent, within the (combined) uncertainty of the corresponding activities at 1σ . Similar conclusions can be drawn comparing the resulting spatial distributions of the activity concentration of ^{238}U progenies (e.g., ^{214}Bi) as well as ^{232}Th progenies that emit gamma-rays (e.g., ^{208}Tl).

Although the sampling and measurement objectives of the lab versus the in situ method are generally different [32,33], a comparison between the results of the two radiometric methods is performed for “in situ validation” purposes. If the activity concentration of any radionuclide of interest along the beach does not vary dramatically, the results of both methods are not expected to differ significantly, irrespective of the strategy, extent

and/or even the quality of sampling [34–36]. On the other hand, when the area of study is highly inhomogeneous in terms of radioactive content and level, e.g., in a beach where erosion locations alternate frequently within the area with accretion ones, or, often, in the wider region around NORM industries, a good sampling strategy and a correctly estimated sampling uncertainty are crucial to ensure the compatibility (equivalency) of the results of the two methods. When the sampling uncertainty is correctly estimated and included together with the analytical uncertainty in the combined measurement and uncertainty, the individual results for a specific location or unit area in the study area—which are produced by applying two or more independent radiomapping/radiometric/radioanalytical methods—are expected to agree within the measurement uncertainty, irrespective of the level of heterogeneity of the area [35]. Finally, in terms of the above reasoning, the results from the in situ mapping methods agreed with the lab-based HRGS analysis of the collected beach sand samples. Therefore, validating the in situ methods supports the reliability of the scanning results which are compatible with those of the lab-based method, with a precision level which is acceptable for relatively fast screening purposes. This agreement is also evident when comparing the ^{40}K -maps in Figures 8–10.

Interestingly, the pattern from the lab-based HRGS results, which is depicted in Figure 10 and reproduced from the respective results of the in situ methods when focusing on the intertidal zone of Legrena Beach, aligns with the hydrodynamic conditions predicted by the TWAC wave model, which shows a gradient in wave energy along the shoreline (see Figure 12). The numerical simulation indicated that the wave amplitude was significantly reduced in the westernmost section (near P1–P7), forming a sheltered zone due to the presence of the breakwater and the rocky barriers. This protection could allow the accumulation of sediments with a higher activity concentration of ^{40}K . In contrast, the lowest activity concentrations of ^{40}K , $^{226}\text{Ra}/^{214}\text{Pb}$, and $^{228}\text{Ra}/^{228}\text{Ac}$ (e.g., 31 ± 7 , 3.1 ± 0.7 , and $2.8 \pm 1.3 \text{ Bq kg}^{-1}$ at P8, respectively) coincide with areas that are directly exposed to wave action, particularly the central part of the beach (P8–P12). The TWAC model predicts an increase in the wave height and energy eastward, with a notable peak near zone D. The above decrease in the activity concentrations with the increasing strength of the wave actions is reasonable, since it could be attributed to the following: a) due to the higher kinetic energy transferred to the sediments, they are sorted in favor of these made of coarser particles, while simultaneously, b) there is usually a differentiation between the radionuclidic fingerprints of fine versus coarse sediment particles, with the latter also exhibiting lower activity concentrations of NOR.

5.2. Statistical Analysis and Cluster Patterns

In the last paragraph of Section 5.1, it was observed that the study area can be divided into subareas containing sediments with either high or low ^{40}K concentrations. These two groups of subareas, classified based on ^{40}K activity concentration, are also reflected in the hierarchical cluster analysis (Figure 13) obtained from the activity concentrations of ^{40}K , $^{228}\text{Ra}/^{228}\text{Ac}$, and $^{226}\text{Ra}/^{214}\text{Pb}$ when the Euclidean distance is used as the clustering metric. This clustering reveals two main distinct groups: one in grey colour, associated with points in the middle of the beach, and the other with two branches in the dendrogram. The red branch groups point to the western part of the beach, and the orange branch groups (P1, P2, P13, and P14), with activity concentrations of ^{40}K ranging from 90 ± 6 to $106 \pm 7 \text{ Bq kg}^{-1}$, are located behind the breakwater and near the mouth of the rivers that stream into the beach.

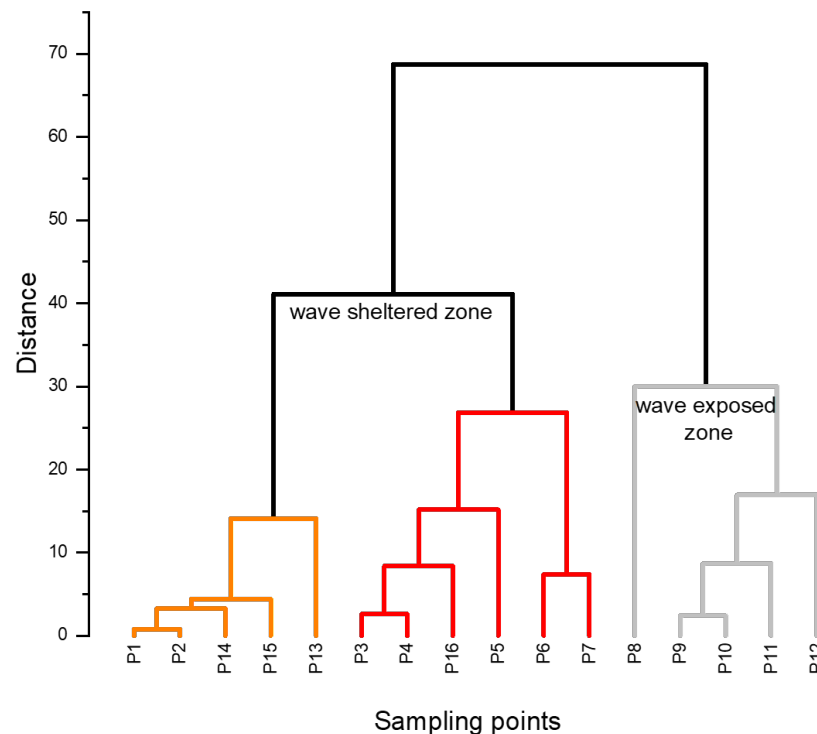


Figure 13. Dendrogram of the cluster analysis of the activity concentrations of ^{40}K , ^{228}Ra and ^{226}Ra , in sediments of Legrena Beach.

Examining the graphs in Figure 10, it is evident that the activity concentrations of $^{228}\text{Ra}/^{228}\text{Ac}$ generally follow the same pattern as ^{40}K ; in contrast, $^{226}\text{Ra}/^{214}\text{Pb}$ does not exhibit the same behaviour. To better understand the variation in natural radionuclides, a correlation analysis was performed between ^{40}K , radium isotopes $^{226,228}\text{Ra}$, and their ratio. Table 1 shows that the correlation between ^{40}K and ^{228}Ra was 0.7795 (p -value = 0.0004), whereas the correlation between ^{40}K and ^{226}Ra is not statistically significant (p -value > 0.05).

Table 1. Correlation coefficient matrix of the activity concentration of ^{40}K , ^{228}Ra , ^{226}Ra , and the ratio $^{226}\text{Ra}/^{228}\text{Ra}$. The p -value obtained for each correlation coefficient is also represented in cursive and is statistically significant when p -values < 0.05.

	^{40}K	^{228}Ra	^{226}Ra	$^{226}\text{Ra}/^{228}\text{Ra}$
^{40}K	1	0.0004	0.0736	0.0004
^{228}Ra	0.7795	1	0.0034	<0.0001
^{226}Ra	0.4591	0.6857	1	0.3387
$^{226}\text{Ra}/^{228}\text{Ra}$	−0.7735	−0.8459	−0.2559	1

Interpolation maps of the activity concentrations of ^{40}K , ^{228}Ra , and ^{226}Ra measured at the sampling points along Legrena Beach, produced using the ArcGIS software 10.8.2., are shown in Figure 14.

The interpolation algorithm used in all mapping cases was the Inverse Distance Weighted (IDW) [37,38]. The study of sediment dynamics was performed by combining the radiometrically determined activity concentrations of natural gamma-ray emitters with the model results. The radionuclide concentrations and their ratios define how zones can be visualized. Furthermore, they can be related to wave forcing on the beach, as well as to land–sea interaction due to intense precipitation events. As proposed in the literature [38], the use of the high-energy gamma-ray emitters among natural radionuclides is adequate for tracing and understanding the sediment dynamics of a beach area. Additionally, the use of thorium isotopes has also been proposed to study sediment dynamics [39,40] and historical trends in case of flooding phenomena that affect—through the streams’ channels—

the coastal zone [30]. Moreover, these isotopes may also be used to identify variations in sediment granulometry. To optimize the radiotracing method for sediment dynamics studies, a normalized process in terms of grain size is recommended in future studies. The comparison of the normalized activity concentrations will support this study to identify zones where sediments are deposited and/or removed from the beach area due to extreme events (e.g., intense precipitation and floods) as well as due to wave interaction with the beach sand area itself.

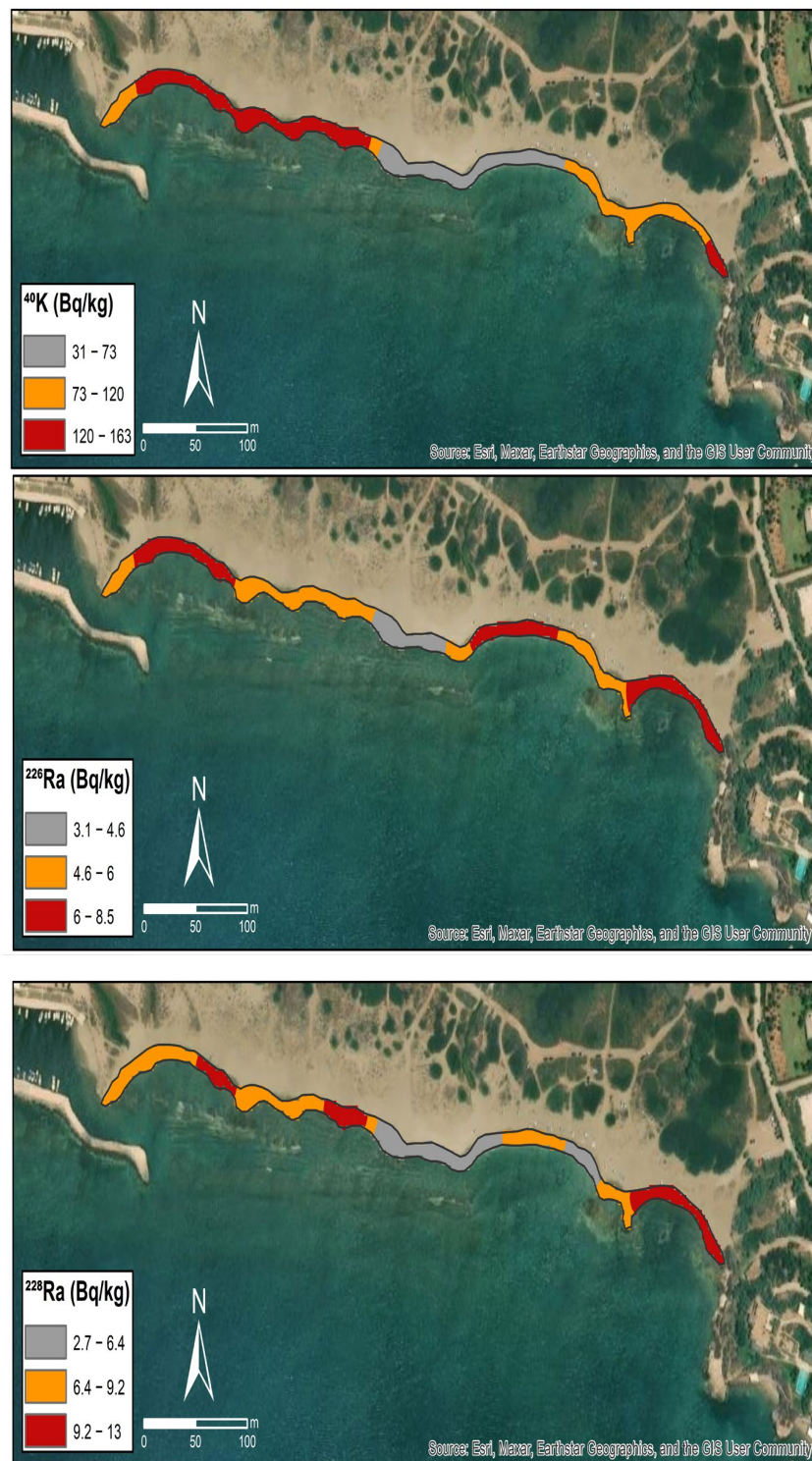


Figure 14. Interpolated maps of the activity concentration of ^{40}K , ^{226}Ra , and ^{228}Ra at the intertidal zone along Legrena Beach, as determined by applying the lab-based HRGS method for the analysis of the collected sand samples (see Figure 3).

A critical component of the validation of the proposed method is the reproduction of the characterization of beach sand movement in terms of sediment dynamics using a hydrodynamic model that incorporates beach morphology (considering not only wave characteristics but also natural and artificial barriers that protect different parts of the beach). The applied model, based on bathymetry and its resolution, does not consider the barriers protecting the beach from wave action between P1–P7 (marine and rocky bar) and P13–P16 (rocky bar). In this case, the model may predict erosion in the open beach (unprotected from wave action, P8–P12) with even greater confidence, which coincides with a decrease in activity concentrations, mainly ^{40}K .

6. Summary—Perspectives

The activity concentrations of natural radionuclides were traced according to existing methods to validate sediment transport processes in Legrena Beach (Attica region, Greece). The in situ gamma-ray spectrometry mapping method was applied repeatedly for the same pilot area, using different instruments each time, to evaluate the role of natural gamma-emitting radionuclides (^{40}K , as well as ^{238}U and ^{232}Th progenies) as tracers of sediment dynamics, and has been proven to be a valuable tool in detecting and understanding or diagnosing these processes in the area of study. The activity concentrations of the studied natural radionuclides on the beach were measured with in-situ methods that were validated with lab-based HRGS analysis of samples from the same area (mainly from the intertidal zone). The radiometric-resulting evaluation data for the sediment dynamics were also validated by a theoretical model predicting the areas with high hydraulic forcing along the shoreline. This validation considers the correlation between specific radionuclides' activity concentrations (i.e., the activities of ^{40}K , ^{226}Ra and ^{228}Ra) and sediment accumulation patterns. The beach morphology (mainly the degree of protection from waves) and the inverse correlation between radionuclide activity and wave height–energy were also discussed. The measured and mapped activity concentrations of NOR, together with the theoretical model results, show spatial variations that are likely related to the sorting processes of sediments. The distribution of radionuclides reflects the selective transport processes of sediment, mainly erosion processes, at the eastern part of the beach.

The in situ methods proved to be valuable for understanding/diagnosing sediment dynamics, using Legrena Beach as a pilot area. The samples that were collected at the protected beach and analyzed by HRGS revealed points with maxima at levels and locations comparable to the results produced by the in situ methods. The ^{40}K activity concentrations in the intertidal zone, as determined by the in situ methods, agree with the respective values from the lab-based HRGS.

The proposed approach could be implemented in other sandy beaches to optimize the in situ methods for determination of the prevailing sediment dynamic patterns. The optimized method would support national and international authorities responsible for the coastal resilience threat due to the storms and sea level rise exacerbated by climate change. The produced radioactivity maps can also support activities related to remediation actions in various aquatic systems (such as bays, ports, and channels) that are affected by sediment transport processes.

Environmental agencies often require independent verification of radionuclide detection, by supporting inter-comparison exercises between spectrometers and compliance with safety thresholds. The comparison of detected spectra from multiple detectors helps pinpoint the origin of radionuclides and ensures accurate assessment of levels of radioactivity. In this work, both the in situ gamma-ray spectrometers exhibit congruent spectral data, demonstrating consistency in the detection and analysis of emitted gamma-rays. This inter-comparison exercise suggests reliable and reproducible measurements of the natural

radioactivity at the beach sand area, reinforcing confidence in the spectrometric results. In the context of environmental radioactivity, this detection systems' comparison may support other applications related to the detection and analysis of naturally occurring radioactive material (including technologically enhanced naturally occurring radioactive material), or contamination by anthropogenic sources (such as accidental or planned releases from nuclear power plants, medical isotopes, fallout from nuclear weapon tests or radiological dispersal devices, etc). In the future, further in situ radiomapping campaigns, focused also in the validation of different analysis and mapping methods (including spectrum decomposition, matrix deconvolution techniques, and deep learning) [41,42], should be implemented to provide consistent data over time in order to have reliable trend analysis, which is critical in assessing the impact of environmental policies (including coastal resilience and/or remediation efforts).

Author Contributions: Data curation, C.T., A.T., R.L.K., D.L.P., D.P.v.B., A.H., V.K., D.M., P.M., S.A., G.E., K.K. and E.G.A.; Formal analysis, D.L.P., R.L.K., A.T., C.M., E.G.A. and D.P.v.B.; Investigation, C.T., A.T., R.L.K., D.L.P., P.M. and D.P.v.B.; Methodology, C.T., S.A., D.L.P., R.L.K., A.T., C.M., D.P.v.B. and A.C.A.-V.; Software, S.A., D.L.P., R.L.K. and C.M.; Supervision, H.A. and C.T.; Validation, A.T., C.T. and D.P.v.B.; Visualization, D.L.P., R.L.K., S.A. and A.C.A.-V.; Writing—original draft, C.T., E.G.A. and G.E.; Writing—review & editing, C.T., C.M., A.T., R.L.K., D.L.P., V.K. and E.G.A.; All authors have read and agreed to the published version of the manuscript.

Funding: This research was not funded by an authority. Some of the tasks were supported by the IAEA, in the frame of the Agency's Coordinated Research Project F22074 as well as the Technical Cooperation Project RER1023. Both IAEA projects did not require this work as deliverable.

Institutional Review Board Statement: This study was conducted in the frame of practical training and a proof-of-concept activity during a coordination meeting in a protected marine area, approved by the Institutional Director of the Institute of Oceanography.

Informed Consent Statement: Informed consent was obtained from all subjects involved in the study.

Data Availability Statement: The data are available on request. The data presented in this study are available on request.

Acknowledgments: The authors would like to acknowledge IAEA for supporting this activity through the Coordinated Research Project F22074, "Development of Radiometric Methods and modelling for measurement of sediment transport in coastal systems and rivers" as well as through the Technical Cooperation project RER1023, supporting various training and workshop events in the European IAEA region. The authors would also like to acknowledge all participants of the IAEA CRP meeting that took place during the week of field experiments, as well as Sofia Papadopoulou (RadioAnalytics S.M. P.C.) for her valuable remarks during draft review. Finally, the authors would like to acknowledge Jovan Thereska being always cheerful to comment on the sediment process that took place in the area of study, as well as for the fruitful discussions we had together for harmonizing data interpretation from the different research groups.

Conflicts of Interest: Author Ronald L. Koomans was employed by the company Medusa Explorations BV. The remaining authors declare that the research was conducted in the absence of any commercial or financial relationships that could be construed as a potential conflict of interest.

References

1. IAEA. *Terminology Used in Nuclear Safety, Nuclear Security, Radiation Protection and Emergency Preparedness and Response 2022 (Interim) Edition*; International Atomic Energy Agency: Vienna, 2022.
2. van Wijngaarden, M.; Venema, L.B.; De Meijer, R.J. Radiometric sand mud characterisation in the Rhine—Meuse Estuary Part B. In situ mapping. *Geomorphology* **2002**, *43*, 103–116. [[CrossRef](#)]
3. van Wijngaarden, M.; Venema, L.B.; De Meijer, R.J.; Zwolsman, J.J.G. Radiometric sand—mud characterisation in the Rhine—Meuse estuary Part A. Fingerprinting. *Geomorphology* **2002**, *43*, 87–101. [[CrossRef](#)]

4. Koomans, R.L.; de Meijer, R.J. Density gradation in cross-shore sediment transport. *Coast. Eng.* **2004**, *51*, 1105–1115. [\[CrossRef\]](#)
5. Nederbragt, G.; Koomans, R.L. Nourishment of the slope of a tidal channel from experiment to practice. In Proceedings of the 5th International Conference on Coastal Dynamics (CD05), Barcelona, Spain, 4–8 April 2005.
6. Venema, L.B.; de Meijer, R.J. Natural radionuclides as tracers of the dispersal of dredge spoil dumped at sea. *J. Env. Radioact.* **2001**, *55*, 221–239. [\[CrossRef\]](#)
7. Bezuidenhout, J. Investigating naturally occurring radionuclides in sediment by characterizing the catchment basin geology of rivers in South Africa. *J. Appl. Geophy.* **2023**, *213*, 105037. [\[CrossRef\]](#)
8. de Meijer, R.J.; Donoghue, J.F. Radiometric fingerprinting of sediments on the Dutch, German and Danish coasts. *Quat. Int.* **1995**, *26*, 43–47. [\[CrossRef\]](#)
9. Komar, P.D.; Wang, C. Processes of Selective Grain Transport and the Formation of Placers on Beaches. *J. Geol.* **1984**, *92*, 637–655. [\[CrossRef\]](#)
10. Koomans, R.L. *Sand in Motion: Effects of Density and Grain Size (PHD)*; RUG: Groningen, The Netherlands, 2000.
11. Tsabaris, C.; Bagatelas, C.; Dakladas, T.; Papadopoulos, C.T.; Vlastou, R.; Chronis, G.T. An autonomous in situ detection system for radioactivity measurements in the marine environment. *Appl. Radiat. Isot.* **2008**, *66*, 1419–1426. [\[CrossRef\]](#)
12. Tsabaris, C.; Androulakaki, E.G.; Ballas, D.; Alexakis, S.; Perivoliotis, L.; Iona, A. Radioactivity Monitoring at North Aegean Sea Integrating In-Situ Sensor in an Ocean Observing Platform. *J. Mar. Sci. Eng.* **2021**, *9*, 77. [\[CrossRef\]](#)
13. Tsabaris, C.; Patiris, D.L.; Adams, R.; Castillo, J.; Henriquez, M.F.; Hurtado, C.; Munoz, L.; Kalpaxis, L.; Verri, M.; Alexakis, S.; et al. In Situ Radioactivity Maps and Trace Metal Concentrations in Beach Sands of a Mining Coastal Area at North Aegean, Greece. *J. Mar. Sci. Eng.* **2023**, *11*, 1207. [\[CrossRef\]](#)
14. Bagatelas, C.; Tsabaris, C.; Kokkoris, M.; Papadopoulos, C.T.; Vlastou, R. Determination of marine gamma activity and study of the minimum detectable activity (MDA) in 4pi geometry based on Monte Carlo simulation. *Environ. Monit. Assess.* **2010**, *165*, 159–168. [\[CrossRef\]](#)
15. Arriola-Velasquez, A.; Tejera, A.; Guerra, J.G.; Alonso, I.; Alonso, H.; Arnedo, M.A.; Rubiano, J.G.; Martel, P. Spatio-temporal variability of natural radioactivity as tracer of beach sedimentary dynamics. *Estuar. Coast Shelf S.* **2019**, *231*, 106476. [\[CrossRef\]](#)
16. Witt, C.; Kopf, A. Submarine Groundwater Discharge in the Nice Airport Landslide Area. *J. Mar. Sci. Eng.* **2025**, *13*, 909. [\[CrossRef\]](#)
17. Tsabaris, C.; Patiris, D.L.; Karageorgis, A.P.; Eleftheriou, G.; Papadopoulos, V.P.; Georgopoulos, D.; Papathanassiou, E.; Povinec, P.P. In-situ radionuclide characterization of a submarine groundwater discharge site at Kalogria Bay, Stoupa, Greece. *J. Environ. Radioact.* **2012**, *108*, 50–59. [\[CrossRef\]](#)
18. Patiris, D.L.; Tsabaris, C.; Maramathas, C.; Alexakis, S.; Roumelioti, S.K. Radioactivity mapping of beach sand by mobile in situ gamma-ray spectrometry. *Hell. Nucl. Phys. Soc. Adv. Nucl. Phys.* **2023**, *30*, 116–123.
19. R Core Team. *R: A Language and Environment for Statistical Computing*; R Foundation for Statistical Computing: Vienna, Austria, 2020. Available online: <https://www.R-project.org> (accessed on 1 January 2019).
20. van der Graaf, E.R.; Limburg, J.; Koomans, R.L.; Tijs, M. Monte Carlo based calibration of scintillation detectors for laboratory and in situ gamma ray measurements. *J. Environ. Radioact.* **2011**, *102*, 270–282. [\[CrossRef\]](#)
21. QGIS Development Team. *QGIS Geographic Information System*; Open Source Geospatial Foundation: Beaverton, OR, USA, 2009; Available online: <http://qgis.org> (accessed on 22 June 2025).
22. IAEA. *Analytical Quality in Nuclear Applications No. IAEA/AQ/19*; International Atomic Energy Agency: Vienna, 2010.
23. Karfopoulos, K.; Domingos, F.; de With, G.; Michalik, B.; Okyar, H.B.; Maramathas, C.; Salpadimos, N.; Potiriadis, C.; Neculae, V.; Ďurecová, A.; et al. Results of the joint IAEA/EEAE Intercomparison exercise on radioanalytical characterization of NORM samples in the European region. *Radiat. Prot. Dosim.* **2025**, *201*, 223–246. [\[CrossRef\]](#)
24. Arriola-Velásquez, A.C.; Tejera, A.; Guerra, J.G.; Geibert, W.; Stimac, I.; C’amara, F.; Alonso, H.; Rubiano, J.G.; Martel, P. ²²⁸Ra and ⁴⁰K as tracers of erosion and accumulation processes: A 3-year study on a beach with different sediment dynamics. *Catena* **2021**, *207*, 105705. [\[CrossRef\]](#)
25. Korres, G.; Ravdas, M.; Zacharioudaki, A.; Denaxa, D.; Sotiropoulou, M. *Mediterranean Sea Waves Reanalysis (CMEMS Med-Waves, MedWAM3 System) Version 1 [Data Set]*; Copernicus Monitoring Environment Marine Service (CMEMS): Brussels, Belgium, 2021. [\[CrossRef\]](#)
26. Escudier, R.; Clementi, E.; Omar, M.; Cipollone, A.; Pistoia, J.; Aydogdu, A.; Drudi, M.; Grandi, A.; Lyubartsev, V.; Lecci, R.; et al. *Mediterranean Sea Physical Reanalysis (CMEMS MED-Currents) Version 1 [Data Set]*; Copernicus Monitoring Environment Marine Service (CMEMS): Brussels, Belgium, 2020. [\[CrossRef\]](#)
27. Villaret, C.; Hervouet, J.-M.; Kopmann, R.; Merkel, U.; Davies, A.G. Morphodynamic modeling using the TELEMAC finite-element system. *Comput. Geosci.* **2013**, *53*, 105–113. [\[CrossRef\]](#)
28. Benoit, M.; Marcos, F.; Becq, F. Development of a third generation shallow water wave model with unstructured spatial meshing. In Proceedings of the 25th International Conference on Coastal Engineering (ICCE’1996), New York, NY, USA, 2–6 September 1996; pp. 465–478.

29. Santoro, P.; Fossati, M.; Tassi, P.; Huybrechts, N.; Piedra-Cuevo, I.; Van Bang, D.P. A coupled wave-current-sediment transport model for an estuarine system: Application to the Río de la Plata and Montevideo Bay. *Appl. Math. Model.* **2017**, *52*, 107–130. [\[CrossRef\]](#)
30. Odom, I.E.; Doe, T.W.; Dott, R.H. Nature of feldspar-grain size relations in some quartz-rich sandstones. *J. Sediment. Res.* **1976**, *46*, 862–870. [\[CrossRef\]](#)
31. JCGM 200:2012; International Vocabulary of Metrology—Basic and General Concepts and Associated Terms (VIM), 3rd ed. Joint Committee for Guides in Metrology, 2012.
32. ISO 18589:3:2023; Measurement of Radioactivity in the Environment-Soil-Part 3: Test Method of Gamma-Emitting Radionuclides Using Gamma-ray Spectrometry. International Organization for Standardization: Geneva, Switzerland, 2023.
33. ISO 18589:7:2013; Measurement of Radioactivity in the Environment-Soil-Part 7: In Situ Measurement of Gamma-Emitting Radionuclides. International Organization for Standardization: Geneva, Switzerland, 2013.
34. ISO 18589:2:2022; Measurement of Radioactivity in the Environment-Soil-Part 2: Guidance for the Selection of the Sampling Strategy, Sampling and Pre-Treatment of Samples. International Organization for Standardization: Geneva, Switzerland, 2022.
35. Ramsey, M.H.; Ellison, S.L.R.; Rostron, P. *Eurachem/EUROLAB/CITAC/Nordtest/AMC Guide: Measurement Uncertainty Arising from Sampling: A Guide to Methods and Approaches*, 2nd ed.; Eurachem, 2019; ISBN 978-0-948926-35-8.
36. Magnusson, B.; Krysell, M.; Sahlin, E.; Näykki, T. *Uncertainty from sampling, Nordtest Report TR 604*, 2nd ed.; Nordtest, 2020; ISBN 978-91-89167-31-5.
37. Achilleos, G.A. The Inverse Distance Weighted interpolation method and error propagation mechanism—Creating a DEM from an analogue topographical map. *J. Spat. Sci.* **2011**, *56*, 283–304. [\[CrossRef\]](#)
38. Gong, G.; Mattevada, S.; O'Bryant, S.E. Comparison of the accuracy of kriging and IDW interpolations in estimating groundwater arsenic concentrations in Texas. *Environ. Res.* **2014**, *130*, 59–69. [\[CrossRef\]](#)
39. Thereska, J. Natural radioactivity of coastal sediments as tracer in dynamic sedimentology. *Nukleonika* **2009**, *54*, 45–50.
40. Yang, W.-F.; Chen, M.; Zhang, X.-X.; Guo, Z.-G.; Li, G.-X.; Ma, Q.; Yang, J.-H.; Huang, Y.-P. Thorium isotopes (^{228}Th , ^{230}Th , ^{232}Th) and applications in reconstructing the Yangtze and Yellow River floods. *Int. J. Sediment Res.* **2013**, *28*, 588–595. [\[CrossRef\]](#)
41. Naeem, N.; Sohail, M.; Ahmed, R.; Masood, S. Application of gamma spectrum analysis techniques for natural radioactivity measurements using NaI(Tl) detector. *Env. Monit Assess.* **2025**, *197*, 418. [\[CrossRef\]](#)
42. Zhao, R.; Liu, L.-Y.; Liu, X.; Liu, Z.-X.; Liang, R.-C.; Ling-Hu, R.-J.; Zhang, J.; Chen, F.-G. Continuum estimation in low-resolution gamma-ray spectra based on deep learning. *Nucl. Sci. Technol.* **2025**, *36*, 23. [\[CrossRef\]](#)

Disclaimer/Publisher's Note: The statements, opinions and data contained in all publications are solely those of the individual author(s) and contributor(s) and not of MDPI and/or the editor(s). MDPI and/or the editor(s) disclaim responsibility for any injury to people or property resulting from any ideas, methods, instructions or products referred to in the content.